JCTC Journal of Chemical Theory and Computation

Microsolvation of Li$^+$ in Small He Clusters. Li$^+$He$_n$ Species from Classical and Quantum Calculations

C. Di Paola, F. Sebastianelli, E. Bodo, I. Baccarelli, and F. A. Gianturco*

Department of Chemistry, University of Rome "La Sapienza" and INFM, Piazzale A. Moro 5, 00185 Rome, Italy

M. Yurtsever

Chemistry Department, Istanbul Technical University, 80626 Maslak, Istanbul, Turkey

Abstract: A structural study of the smaller Li$^+$He$_n$ clusters with $n \leq 30$ has been carried out using different theoretical methods. The structures and the energetics of the clusters have been obtained using both classical energy minimization methods and quantum Diffusion Monte Carlo. The total interaction acting within the clusters has been obtained as a sum of pairwise potentials: Li$^+$−He and He−He. This approximation had been shown in our earlier study to give substantially correct results for energies and geometries once compared to full ab initio calculations. The general features of the spatial structures, and their energetics, are discussed in details for the clusters up to $n = 30$, and the first solvation shell is shown to be essentially completed by the first 8−10 helium atoms.

I. Introduction

The study of the nanoscopic forces which act within small aggregates of weakly interacting particles, especially within assemblies containing helium atoms, has received a great deal of attention in the past few years[1−4] because of the broad range of phenomena that can be probed under the very special conditions provided by the He nanodroplets as containers of atoms or molecules. They are, indeed, ultracold homogeneous matrices where the corresponding spectra often reach very high resolution due to the superfluid properties of the helium droplet.[5]

The possibility of causing electronic excitation and/or ionization of the dopant species can offer additional ways of probing the modified interaction between the new ionic species and the gentle matrix of the helium droplets[4] since the ensuing distribution surrounding the molecular impurity is usually markedly deformed as a consequence of the electrostriction effects on the solvent brought on by the induction forces between the charged dopant and the helium

atoms in the droplet:[6−8] It simply means that the local density of the quantum solvent is going to markedly increase around the cationic dopant. The analysis of such effects in the case of lithium-containing impurities has been particularly intriguing because of the expected simplicity of the electronic structures involved and, at the same time, the unusual bonding behavior of such systems. Furthermore, experiments in which the droplet was ionized after capture of Li atoms[9] have revealed a wealth of newly formed species such as Li$^+$, Li$_2^+$, and LiHe$^+$ which are produced during droplet fragmentation and evaporation thereby triggering the corresponding analysis of structure and bonding behavior from theory and computations.

In a previous computational investigation[1] on the interaction of Li$^+$ with n helium atoms, with n varying from 1 to 6, we have shown, in fact, that the energy optimized structures of the clusters were largely determined by two-body (2B) forces, with the many-body effects being fairly negligible for determining the final geometry of those small aggregates. In the present study we have therefore decided to analyze in greater detail the quantum states and binding energies of the larger structures of Li$^+$ impurities within the

* Corresponding author fax: +39-05-49913305; e-mail: fa.gianturco@caspur.it.
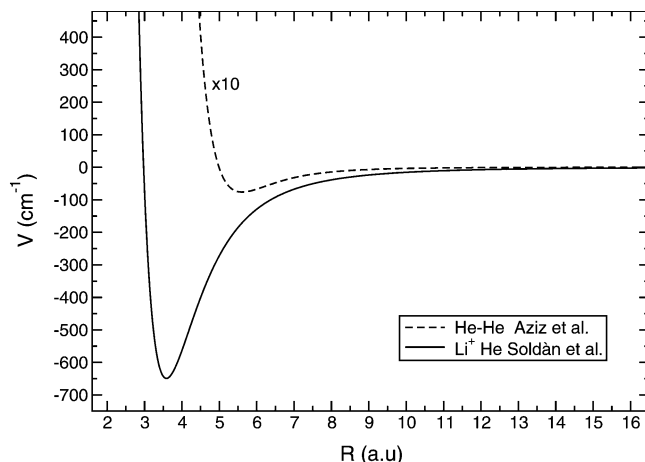
Figure 1. Comparison of the LiHe⁺ potential from ref 17 and the He−He one from ref 18. The He−He potential has been multiplied by ten.

helium droplets in order to extend our computational knowledge on such species.

The next section briefly describes the LiHe⁺ Potential Energy Curve (PEC) used here. The results for the trimer ground state are given and discussed in section III, where we report the features obtained using the distributed Gaussian functions (DGF) method[10−13] and the quantum Diffusion Monte Carlo (DMC) method,[14] in comparison with the values obtained via a classical minimization procedure. Section IV extends the discussion to the larger species, whose energetics and structural features, both obtained with DMC and classical methods, are analyzed.

II. The Pairwise Potentials

The actual potential energy curve (PEC) for Li⁺He has been studied before because of its interest in modeling low-energy plasmas.[15] Alrichs and co-workers suggested a model potential as a variant of the Tang-Toennies model[16] which we shall here call the ATT potential. More recent calculations of Soldán et al.[17] employed a CCSD(T) treatment and used the aug-cc-pV5Z basis set. Recently, we have also carried out a new set of calculations on these clusters[1] using the MP4 method and the cc-pV5Z basis set. The three potentials provide very similar values of ZPE that are respectively 131.09, 129.18, and 128.75 cm⁻¹, values which roughly correspond to 20% of the well depth.

For the He₂ dimer we have employed the semiempirical potential (LM2M2) of Aziz and Slaman:[18] in Figure 1 we sketch the two pair potentials used in our calculations. The two potentials are completely different: the Li⁺−He one is dominated by electrostatic and induction forces, while the He−He interaction is much weaker and purely van der Waals in nature.

As we mentioned above, the full interaction that acts in the M⁺Rg$_n$ clusters can be approximated by a sum of pairwise potentials. The main source of error in this model is due to the absence of the repulsive interactions between the induced dipoles on the helium atoms, especially those that are located near the ionic center. These interactions, however, can be taken to be very small for rare gas atoms and especially for helium partners. For example, in ref 19 for the analogous situation of the anionic dopant Cl⁻ in Ar clusters it has been shown that the inclusion of the leading terms of such three-body forces does not alter substantially the energetics and the structure of the clusters: in ref 1 we have discussed and confirmed this feature for the system analyzed here. Furthermore, since the charge delocalization in Li⁺−He$_n$ is very small[20] and the interaction is mostly determined by "physical" forces (charge/induced multipole) rather than by "chemical" effects, all the helium atoms that are attached directly to the ionic center can be considered to be equivalent because there is no detectable tendency for the latter to preferentially form chemically bound structures with only a subset of such adatoms, a fact which would therefore differentiate some of the binding effects with respect to those in the rest of the cluster.

III. An Outline of the Computational Tools

A. The Classical Optimization. The total potential in each cluster is described by the sum of pairwise potentials, and searching for the global minimum in this hypersurface V_{TOT} will give us the lowest energy structure for each aggregate from a classical picture viewpoint. All the classical minimizations were carried out with a modified version of the OPTIM code by Wales.[21] This code is based on the eigenvector following method. The basis of this method is the introduction of an additional Lagrange parameter into a "traditional" optimization framework,[22] which seeks to simultaneously minimize in all directions. All searches were conducted in Cartesian coordinates using projection operators to remove overall translation and rotation following Baker and Hehre.[23] Analytic first and second derivatives of the energy were employed at every step, and the resulting stationary point energies and geometries are essentially exact for the model potential in question. The details of the method as applied in our group have been given before and therefore will not be repeated here[21,24−26]

B. The Quantum Monte Carlo Calculations (DMC). The Diffusion Monte Carlo Method has been extensively discussed in a number of papers (refs 27−29 and references therein) and therefore will not be repeated here.

In our implementation a random walk technique is used to solve the diffusion equation where a large number of random walkers is propagated with time steps $\Delta\tau$ starting from an arbitrarily chosen initial distribution. The ground-state energy E_0 is obtained by averaging $E_L(\mathbf{r})$ over the final mixed distributions $f(\mathbf{r},t) = \psi_T(\mathbf{r},t)\psi(\mathbf{r},t)$:

$$\langle E_L \rangle = \frac{\int E_L(\mathbf{r})f(\mathbf{r},\tau_f)\,d\mathbf{r}}{\int f(\mathbf{r},\tau_f)\,d\mathbf{r}} = \frac{\int \psi_0(\mathbf{r})\hat{H}\psi_T(\mathbf{r})\,d\mathbf{r}}{\int \psi_0(\mathbf{r})\psi_T(\mathbf{r})\,d\mathbf{r}} = E_0 \quad (1)$$

The energy is therefore affected by a bias due to the use of a mixed distribution. The bias is however minimized by using very long propagation time and very short time steps. Expectation values of position operators $\hat{A}(\mathbf{r})$ are also given by averaging over $f(\mathbf{r})$, a procedure that leads to biased distributions. However, we believe that the bias does not modify the qualitative picture of the present calculations especially because whenever our spatial distributions are

Microsolvation of Li⁺ in Small He Clusters

J. Chem. Theory Comput., Vol. 1, No. 5, 2005 **1047**

compared with those from other quantum calculations (where possible) and with classically minimized structures, they are found to be in remarkable agreement with each other as we shall discuss further below.

The trial function used here for the He−He pairs is a product of trial wave function

$$\Psi_T = \prod_{i,j \in He} \exp\left(-\frac{p_5}{R_{ij}^5} - \frac{p_2}{R_{ij}^3} - p_0 \log R_{ij} - p_1 R_{ij}\right) \quad (2)$$

where the values of the coefficients have been taken by ref 30. The trial function for the Li⁺−He pair has been chosen as a Gaussian function centered around the energy minimum of the relative interaction. However, to adjust each trial wave function to the size of the larger clusters, its parameters have been chosen so that they make it increasingly more delocalized as the number of adatoms is increased. Our trial functions are available on request from the correponding author.

C. The Distributed Gaussian Functions (DGF) Expansion. The DGF method[10−13] is a variational approach developed in our group which solves the trimer bound state problem written in terms of the atom−atom coordinates by employing a large ensemble of distributed Gaussian functions as a basis set.

First of all, the Hamiltonian for a triatomic system is expressed in terms of atom pair coordinates R_1, R_2, and R_3, i.e., in terms of the distances between each pair of atoms along which the Gaussian functions are distributed (see ref 12 for the expression of the Hamiltonian for a triatomic system with an impurity).

The total potential for the trimer is assumed to be the sum of the three two-body potentials as discussed previously, and the calculations are carried out for a zero total angular momentum. The total wave function for the vth vibrational states is then expanded in terms of symmetrized basis functions

$$\Phi_v(R_1,R_2,R_3) = \sum_j a_j^{(v)} \phi_j(R_1,R_2,R_3) \quad (3)$$

with

$$\phi_j(R_1,R_2,R_3) = N_{lmn}^{-1/2} \sum_{P \in S_2} P[\varphi_l(R_1)\varphi_m(R_2)]\varphi_n(R_3) \quad (4)$$

for the two-identical-particle system. Here, j denotes a collective index such as $j = (l \le m;n)$, N_{lmn} is a normalization constant expressed in terms of the overlap integrals $s_{pq} = \langle \varphi_p | \varphi_q \rangle$, and P is the permutation operator between the two helium atoms. Each one-dimensional function φ_p is chosen to be a Gaussian centered at the R_p position

$$\varphi_p(R_i) = \sqrt[4]{\mathrm{frac}2A_p\pi}e^{-A_p(R_i-R_p)^2} \quad (5)$$

With the DGF approach we can obtain several indicators on the spatial behavior of the bound states of the systems (the root mean value of the square area, the average of the cosine value−and the various moments−of any angle, etc.), along with several probability distribution functions such as the pair distribution function

$$D^{(v)}(R_1) = \int \int |\Phi_v(R_1,R_2,R_3)|^2 \, dR_2 \, dR_3 \quad (6)$$

The selection of a suitable set of Gaussian functions and their distribution within the physical space where the bound states are located is obviously of primary importance in order to finally obtain converged and stable results. We extensively experimented with different sets obtained by changing the number and location of the DGF depending on the features of the 2B potentials employed. The details of the basis set employed for the Li⁺He₂ system are specifically given in the following section.

IV. The Li⁺He₂ Trimer

Together with the classical optimization and the DMC calculations, we further carried out the analysis of the properties of the trimer Li⁺He₂ using the DGF method. We employed an optimized DGF basis set in order to obtain well-behaving total wave functions at the triangle inequality boundaries (for further details see ref 31). The Gaussian functions are distributed equidistantly along the atom−atom coordinates starting from 2.55 a_0 and out to 9.18 a_0 with a step of 0.17 a_0, a choice which ensures converged results within about 0.1 cm⁻¹ (0.01% of the total ground-state energy). In Table 1 we report the results obtained with DMC and DGF methods: they are seen to be in good agreement with each other. Due to the addition of the second light He atom, the Zero Point Energy (ZPE) of the trimer is about twice the ZPE value for the isolated dimer ion. The two ZPE values remain very similar as percentage values of the overall interaction showing that the Li⁺ impurity strongly affects the features of the cluster, as expected from the involved potentials, while the additional helium atom has little effect on the bonding features. The ionic system, as expected, does not present the typical high degree of delocalization shown in pure He clusters (the ZPE for He₃ is more than 99% of its total well depth[32]) or by doped He aggregates with weakly bound impurities as, e.g., H⁻, for which the impurity is clearly located outside the cluster (the ZPE for H⁻He₂ is 90.66%[24]). Hence, we expect the Li⁺−He₂ trimer (and its larger clusters) to behave in a different way with respect to the more weakly bound neutral He clusters and thus presume that the classical description of the ionic structures should give us realistic indications on the structure and energetics of such systems (as it was the case in, e.g., the H⁻Ar_n clusters that we studied earlier[25]).

We therefore begin by looking at the average values of the radial distances and angles (see Table 1) which, together with the corresponding standard deviations, describe the ground state of the trimer and clearly confirm its having a rather floppy structure: on the other hand, the Li⁺ species still is undoubtedly seen by our calculations to coordinate the two He atoms at a distance determined within 0.3 a_0. Information on the overall geometrical features of the trimer is further gained from the radial and angular distributions shown in Figure 2, where the values obtained with the classical optimization are also reported as vertical lines. DMC and DGF results are substantially coincident, and the small differences are mainly due to the bias contained in our DMC distributions. We notice that the floppiness of the system is

Table 1. Comparison of the Results for the Ground State of $(LiHe_2)^+$ Obtained with Both DMC and DGF Methods[a]

	$E_{v=0}$	ZPE (%)	r_{He-He}	r_{He-Li^+}	$\theta_{\widehat{He}}$	$\theta_{\widehat{Li}^+}$	$\sqrt{\langle S^2 \rangle}$
DMC	-1041.7 ± 0.68	20.24	6.59 ± 0.81	3.83 ± 0.32	28.43 ± 12.20	123.88 ± 24.01	5.54 ± 1.84
DGF	-1042.45	20.18	6.69 ± 0.73	3.75 ± 0.32	26.94 ± 17.69	127.36 ± 27.99	5.24

[a] The energies are in cm^{-1}, the distances in au, the angles in degrees, and the areas S in $au.^2$ The ZPE is expressed as a percentage of the total well depth for the trimer $D_e = 1306.02$ cm^{-1} (from classical optimization).
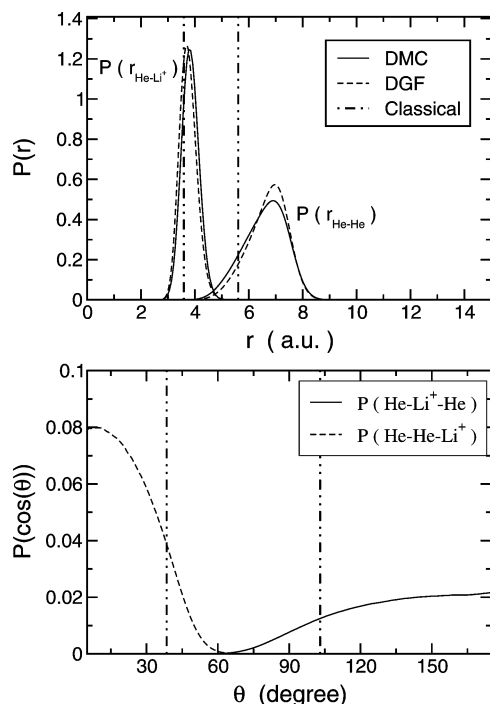
Figure 2. The radial distribution functions for the Li^+He_2 calculated via the DMC (solid line) and the DGF (dashed line) methods. In the upper panel we report the pair distribution functions of the relative atom−atom distances, while the lower panel shows the distribution functions for the internal angles. The (r,θ) values obtained classically are given as vertical lines in the two panels.

particularly evident when looking at the distribution function related to the He−He distance, whose standard deviation is more than twice as large as than the one for the Li^+−He bonds. The classical values obtained in the structure optimization are also closer to the quantum average values obtained for the Li^+−He distances.

In the classical description we do find that the ground state of the trimer is depicted by an isosceles triangle, with the two shorter sides associated with the two Li^+−He distances and a longer one corresponding to the He−He distance. On the other hand, the real quantum system cannot be described by one single structure only, and its distribution functions correctly show a delocalized triatom with a dominant contribution from the collinear arrangement. The image of a structure with the Li^+ coordinating the two He atoms at a rather well-defined distance (notice the compact distribution function related to Li^+−He distances) is not completely lost in the quantum description, meaning that the presence of the strong ionic forces from Li^+ is reducing the degree of delocalization which is always present in the pure He aggregates. This change determines the more rigid structure of the system in the sense that now the He atoms are more

strongly coordinated directly to the Li^+ impurity (see the next section on the larger clusters).

We carried out an additional analysis of the structural features of the trimer by taking advantage of the DGF pseudoweights,[10] which allow us to pictorially describe the trimer in terms of types of triangular arrangements. In the upper panel of Figure 3 we thus report the total number of the employed basis set functions, grouped according to the triangular family to which they belong, and in the lower panel of the same figure we report the 'weight' of the dominant families when describing the ground state of the trimer. We can thus easily identify the most important arrangement to be given by the 'flat' isosceles, the collinear (with the impurity in the middle), and the scalene triangles, while all other possibilities do not contribute in a significant way. Again, we find that we cannot associate the system to one unique structure. while the marked delocalization features are now mainly related to the He−He binding and less to the Li^+−He ionic forces; hence we see that a conventional structure with the Li^+ coordinating the two He atoms can still be qualitatively identified. In the next section we shall further discuss how the situation evolves with the addition of more He atoms and to which extent the classical results can be still seen to qualitatively correspond to the quantum description of their structures surrounding the ionic dopant.

V. Energetics and Structures of Li^+−He_n ($3 \leq n \leq 30$) Clusters from Quantum and Classical Calculations

We start now to discuss the energetics and the geometrical features of the larger Li^+He_n clusters with $n \geq 3$. Up to $n = 20$, in fact, it was still possible to also carry out quantum DMC calculations which are not too demanding in terms of CPU-time. Hence, for clusters of such a size we can make a direct comparison between our quantum findings and the classical optimization results we obtained via the combination of the OPTIM procedure[21] with a random search for the minimum energy structures (see for details refs 25 and 26). In Table 2 we report the results for the energetics. The left part of that table shows the minimum potential energies obtained by means of the classical optimizations (column labeled 'classical') in comparison with the corresponding DMC ground-state energies (column labeled 'quantum'). The differences between the two sets of values are due to the ZPE effects of the nuclear motions: in the third column we also display the ZPE value for each cluster as a percentage of the well depth. The amount of the ZPE effects increases as the cluster grows, since the increasing addition of He atoms brings the ZPE percentage from about 20% for Li^+-He_2 to more than 40% for the last cluster studied here with the quantum DMC method (Li^+He_{20}). On the right part of Table 2 we report the total energies relative to the loss of

Microsolvation of Li⁺ in Small He Clusters

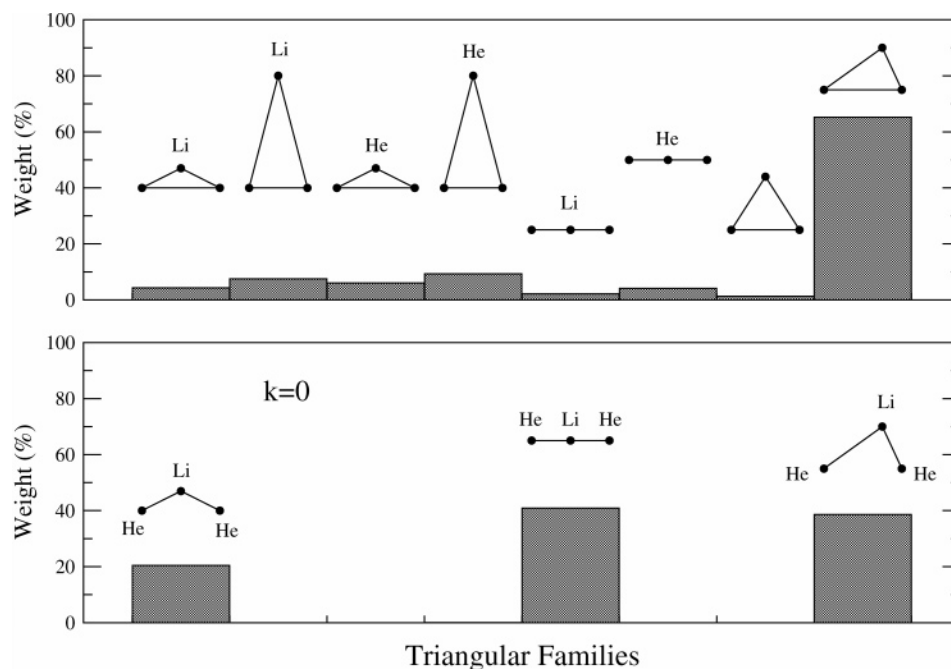*J. Chem. Theory Comput., Vol. 1, No. 5, 2005* **1049**

Figure 3. DGF description of the ground state of the Li⁺He₂ in terms of triangular families. In the upper panel we report the relative weights of the triangular groups of basis functions (as percentage with respect to their total number) which correspond to the different types of triangular configurations sketched in that panel. In the lower panel we show the three configurations that contribute the most to the ground state of the trimer.

Table 2. Minimum Total Energies and Single-Particle Evaporation Energies Using Classical and Quantum Treatments for the Nuclear Motion[a]

	V^{TOT}			ΔE_{evap}	
n	classical	quantum	ZPE (%)	classical	quantum
2	−1306.0	−1041.7 ± 0.7	20.2	656.8	521.1 ± 0.7
3	−1970.5	−1556.3 ± 0.8	21.0	664.4	514.6 ± 1.5
4	−2640.1	−2038.1 ± 2.9	22.8	669.6	481.7 ± 3.7
5	−3287.0	−2474.1 ± 4.6	24.7	646.9	436.1 ± 7.5
6	−3940.2	−2895.3 ± 10.3	26.5	653.1	421.1 ± 14.9
7	−4281.4	−3000.7 ± 14.7	29.9	341.2	105.4 ± 25.0
8	−4627.6	−3161.5 ± 23.5	31.7	346.2	160.8 ± 38.2
9	−4789.3	−3234.3 ± 9.5	32.5	161.7	72.8 ± 33.0
10	−4936.0	−3271.2 ± 19.5	33.7	146.7	36.9 ± 29.0
14	−5284.2	−3292.4 ± 18.1	37.7	88.4	5.3 ± 37.6
20	−5785.6	−3432.5 ± 56.1	40.7	72.2	23.3 ± 74.2

[a] ZPE (%) means: $[(V^{TOT}_{classical} - V^{TOT}_{quantum})/V^{TOT}_{classical}]\cdot 100$. ΔE_{evap} means: $-[V^{TOT}(Li^+(He)_n) - V^{TOT}(Li^+(He)_{n-1})]$ the quantum evaporation energy for $n = 14$ has been calculated using the formula $E_{evap}(14) = (V^{TOT}(10) - V^{TOT}(14))/4$ and for $n = 20$ $E_{evap}(20) = (V^{TOT}(14) - V^{TOT}(20))/6$.

one He atom between the pairs of Li⁺He$_n$ and Li⁺He$_{n-1}$ clusters, calculated both with the classical and quantum methods. We notice that the evaporation energy is drastically reduced when passing from the cluster with $n = 6$ to that with $n = 7$ and correspondingly the ZPE percentage value increases most markedly (more than 3%). We can then surmise that the structure with $n = 6$ is a particularly stable cluster as we shall further discuss below.

The data presented in Table 2 are pictorially reported in the two panels of Figure 4 where the energies are plotted as functions of the number n of He atoms in each cluster. From the lower panel of Figure 4 we can see the similar behavior shown by the ΔE_{ev} values up to $n = 6$, while for $7 \leq n \leq$

10 both classical and quantum effects make the two curves show a marked drop in values. The single He atom evaporation energies, $\Delta E_{ev} = -[E(Li^+He_n) - E(Li^+He_{n-1})]$ (filled-in circles for the classical calculations and open square for those obtained with the DMC method), are plotted up to $n = 30$ (DMC results up to $n = 20$): again the two curves show very similar behavior, both presenting the same abrupt energy drop at $n = 7$ and $n = 9$. In contrast with what we found in our analysis of H⁻He$_n$ clusters,[24] the steplike structure shown by the classical treatment is now also present in the quantum calculations. Given such a correspondence between the classical and quantum description for these smaller clusters it then becomes reasonable to try to explain the sudden energy jumps of Figure 4 by looking at the lowest energy structures found with the classical minimizations (see Figure 5). In that figure we also report the corresponding symmetry groups, the total energy (in cm⁻¹), and the relevant distances between atoms (in au). We therefore see that the Li⁺He₆ has the very symmetrical octahedral geometry (see the second panel in the upper part of the figure) where all the He atoms are equivalently coordinated to the central Li⁺ at a distance very close to the R_{eq} (3.58 a_0) of the Li⁺He PEC. On the other hand, when moving to the Li⁺He₇, the repulsive forces acting between the rare gas species do not allow any more for such a symmetrical arrangement around the Li⁺ ion, and the net effect is that of decreasing the energy contributions from the interactions between each He atom and the positive ion, i.e., the Li⁺He distance becomes larger, as one can see in Figure 5 from the reported R_{LiHe} values. Similar reasoning can be applied to explain the second energy step between $n = 8$ and $n = 9$: the evaporation energy gives the mean value of the energy necessary to remove any of the He atoms, and the presence of a nonequivalent rare gas
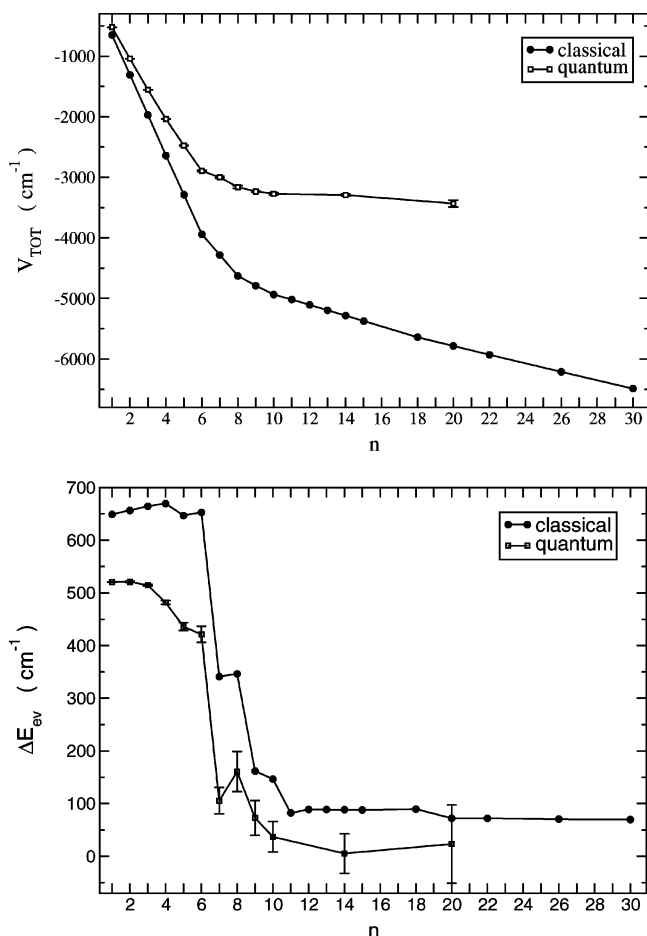
Figure 4. Upper panel: total energies (in cm^{-1}) as a function of the number n of helium atoms in Li^+H_n from classical optimizations (filled-in circles). Lower panel: single helium atom evaporation energies, $\Delta E = -[E(Li^+He_n) - E(Li^+He_{n-1})]$ in cm^{-1}, as a function of the number n of helium atoms in Li^+He_n from the classical optimizations (filled-in circles). The quantum results are given in both panels in open squares showing their corresponding numerical level of confidence.

atom in the apical position in Li^+He_9 (see second panel in the lower part of Figure 5) causes a significant decrease of the evaporation energy with respect to its value for the Li^+-He_8 cluster. Finally, for Li^+He_{10} the lowest energy structure we obtained with the classical minimization corresponds to the symmetrical *bicapped square antiprism* geometry. Hence, by using the classical geometries and energy minimization procedures, we found three relatively more stable structures for clusters with $n = 6, 8,$ and 10, in correspondence with symmetrically compact structures. We therefore have here a relatively complex situation in which we clearly see the formation of a very stable "shell" with 6 He atoms, but, nevertheless, we also see the closing of two successive "shells" at $n = 8$ and $n = 10$. After the first ten He atoms have been placed around the ionic impurity in the bicapped antiprims geometry, the cluster growth is chiefly driven by weaker and essentially dispersive forces. While these results stem clearly from the classical calculations, the quantum evaporation energies are affected by large errors for $n > 6$, and therefore the quantum structures of the cluster for $n > 6$ are less easy to establish.

The correspondence between classical and quantum structural pictures is fairly well reproduced if we now compare the quantum distribution functions with the classical results for the relative distances and angles. In Figure 6 we report the DMC atom−atom distribution functions for the Li^+−He and He−He distances within each Li^+He_n cluster, normalized to the total number n of possible 'connections' between Li^+ and He atoms (solid lines) and to the total number $N = n(n − 1)/2$ possible 'connections' between the n He atoms (dashed lines). In this way we can make a direct comparison between the quantum calculations and the lowest energy geometrical structures obtained with the classical optimizations where the conventional picture of direct bonds existing between localized, pointlike, partners can be used. In that figure we also report the classically optimized distances: we have grouped together sets of close values and have given as horizontal bars their statistical standard deviations: each set has a height proportional to the number of distances which have the same value. Finally, the displayed numbers are the values of the integration along r for each broad peak in the quantum distribution functions and represent the number of connections within atoms which are in the given distance range under each integration. For some of the larger clusters the results of the integration depended slightly on the choice of the fitting functions (essentially we have used an asymmetric Gaussian for each peak), and therefore we have reported an interval of possible values. The numbers reported above each quantum distribution should be directly compared to the height of the classical vertical lines. In Figure 6 we report the results for four selected clusters ($n = 4, 6, 7, 10$) which we shall use in our discussion: we also obtained similar results for all the other clusters. When we look at the panel showing the Li^+He_4 clusters in the upper left of Figure 6, we see that the DMC distribution function for the Li^+−He distance peaks at 3.88 au, while the classical distances are represented by one 'stick' at 3.59 au whose height is 4, equal to the value of the area under the quantum distribution (solid line); we see also that the DMC distribution function for the He−He distance peaks at 6.13 au, while the classical distances are represented by one 'stick' at 5.85 au whose height is 6 (which is the value of $N = n(n − 1)/2$, with $n = 4$) a number which is indeed equal to the value of the area under the quantum distribution (dashed line). For the larger clusters (see the other panels of the same figure) the number of distinct sets of distances increases, but still the agreement between classical and quantum findings concerning the number of corresponding distances remains very good. Although the mean values are different as a consequence of the very diffuse behavior of the wave functions, we can clearly see that the classical results essentially provide the same qualitative structural picture. For example in the panel referring to Li^+He_{10} we see clearly also from the quantum calculation the formation of the first shell of 8 atoms and the second shell constituted by only two atoms. To compare even more in detail the classical and quantum results, we report in Figure 7 the DMC angular distribution functions $P(\theta)$ for the angles centered at the Li^+ ion and at any of the He atoms together with the results from classical optimization: we see again that the
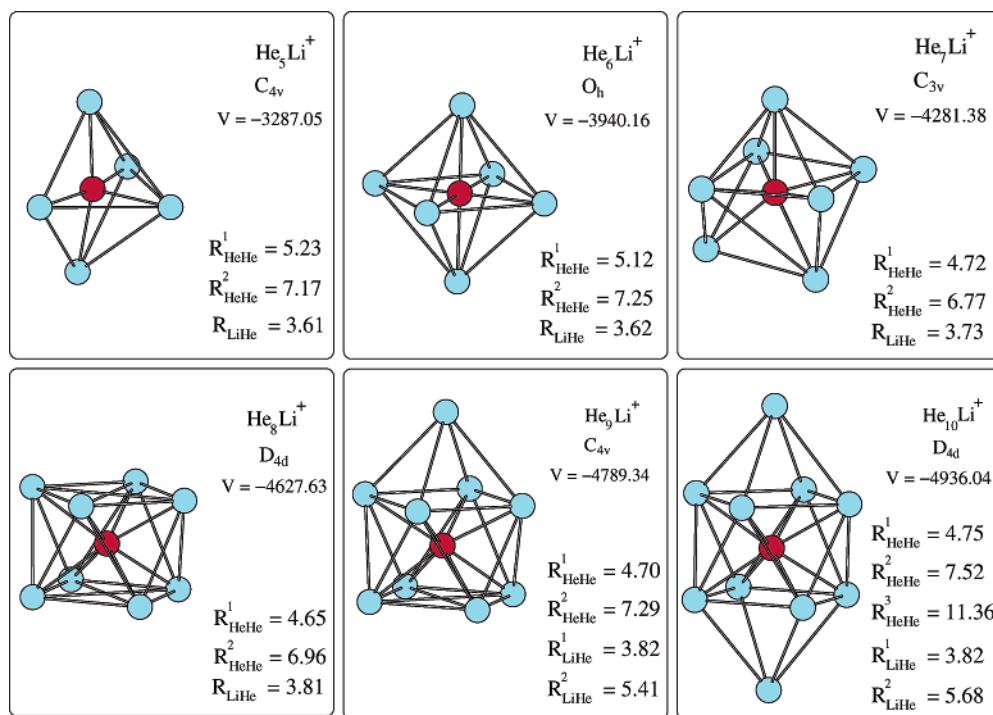
Microsolvation of Li$^+$ in Small He Clusters

J. Chem. Theory Comput., Vol. 1, No. 5, 2005 **1051**

Figure 5. Optimized lowest energy structures obtained with the classical minimizations for Li$^+$He$_n$ with n from 5 to 10.
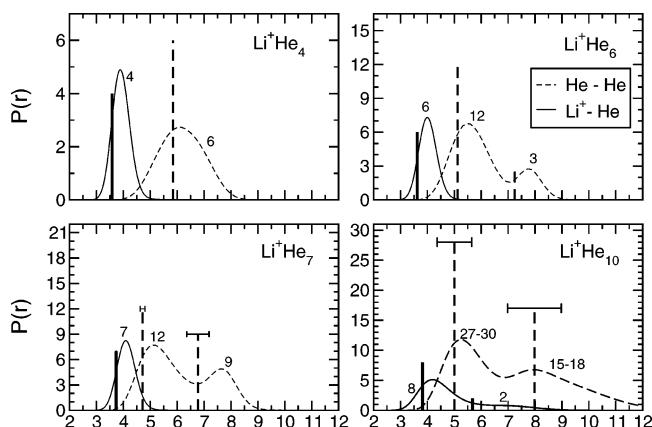

Figure 6. Radial distribution functions of the atom−atom relative distances $P(r)$, normalized to the number of 'connections' between the atoms in each cluster, as a function of the distance r (in au). DMC calculations for the Li$^+$He$_n$, $n = 4$, 6, 7, 10. In all panels the solid lines are for the Li$^+$−He distances, while the dashed ones refer to the He−He distances. The vertical lines indicate the computed mean values of the atom−atom distances (solid lines for Li$^+$−He and dashed lines for He−He) of the optimized structures from the classical calculations, with their height showing the number of bonds associated with that distance (marked also by its spread value on top of each "stick"). The presented numbers in each panel give the corresponding quantum density of bonds within each computed profile.

Figure 7. Angular distribution functions $P(\theta)$, obtained with the DMC calculations for the Li$^+$He$_n$, $n = 4$, 6, 7, 10. In all the panels the solid line is for the He−He−Li$^+$ angles, and the dashed line is for the He−Li$^+$−He angles. The vertical lines indicate the various mean values of the angles (solid lines for He−He−Li$^+$ and dashed lines for He−Li$^+$−He) of the optimized structures given by the classical calculations. The notation is the same as in Figure 7

agreement between quantum and classical values (vertical lines) indeed remains very close, at least at the qualitative level.

These findings allow us to make further comments on the microsolvation process that occurs when the Li$^+$ is inserted in a small He cluster. Both the classical and the quantum treatments concur in locating the Li$^+$ impurity inside the He$_n$
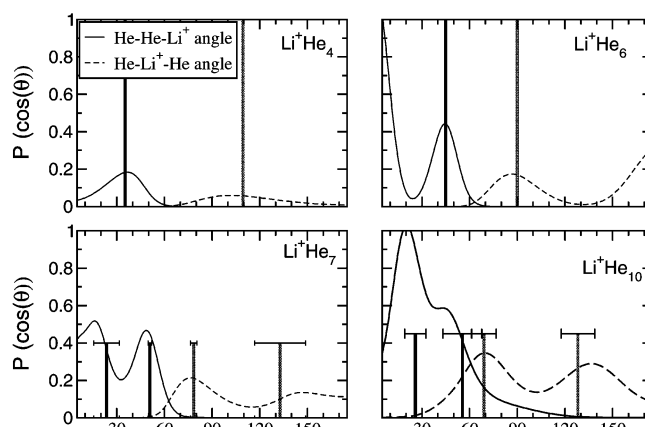
moiety as one can clearly see from Figure 8 where we report the DMC distribution functions $P(r)$ of the Li$^+$ (solid lines) and of the He atoms (dashed lines) from the geometrical center of each Li$^+$He$_n$ cluster. This quantity is defined as

$$\mathbf{r}_{gc} = \frac{1}{N}\sum_{i=1}^{N}\mathbf{r}_i \qquad (7)$$

where N runs over the total number of atoms in the cluster. The Li$^+$ is always closer to the geometrical center with respect to the He atoms, and when the cluster size increases the corresponding distribution functions have reduced over-
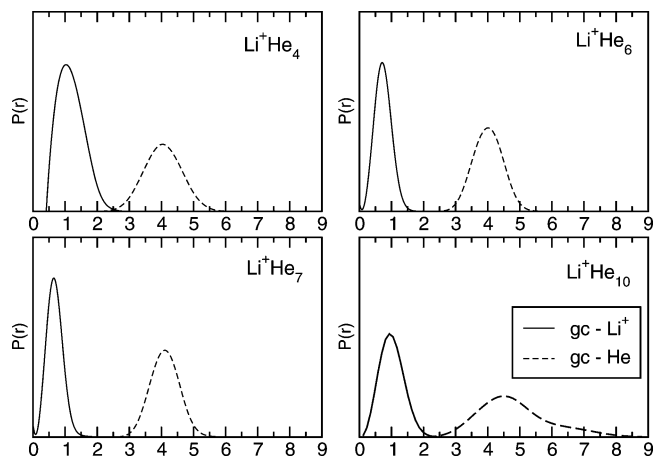
Figure 8. DMC radial distribution functions of the distances of the He atoms (dashed lines) and of the Li$^+$ (solid lines) from the geometrical center (gc) for selected clusters as functions of the distance r (in au). The density distributions are normalized so that the area under them is unitary.

lap, thereby showing that the cluster growth is accompanied by a slow "dropping" of the Li$^+$ toward the geometrical center of the latter, although the process is by no means monotonic with cluster size.

Finally, we carried out classical optimizations for larger clusters Li$^+$He$_n$ ($n = 11-15$, 18, 20, 22, 26, 30) in order to better confirm what we have observed in the smaller ones; the lowest energy geometries for a selection of them are reported in Figure 9. For all the clusters under inspection the growth occurs around the highly symmetric Li$^+$He$_{10}$ core represented by the bicapped square antiprism polyhedron enclosing the Li$^+$ impurity and drawn with thicker lines in the figure. The additional He atoms are now being placed

further away from the impurity without perturbing the structure of the Li$^+$He$_{10}$ moiety which therefore seems to constitute the last solvation shell of the atomic ion. We expect that the He atoms outside the shell will be characterized by a greater delocalization and weaker interactions with the central Li$^+$ that the less shielded inner core of 10 atoms. From now on we expect, therefore, that the cluster will grow by adding more solvent atoms in a nearly isotropic fashion driven mainly by He–He interaction, and we surmise that the binding energies of each atom will become increasingly similar to those of a pure He cluster. Correspondingly, the evaporation energy (see Figure 4) now shows a markedly different behavior with respect to what happens in the smaller clusters with $n \leq 10$: the steplike feature disappears, to be substituted by a plateau giving us the average energy needed to remove one of the nearly equivalent external He atoms.

This expected result is also shown by the quantum calculations (see Figure 4, lower panel) and is also borne out by the corresponding quantum distributions of the helium adatoms given by the data of Figure 10, where our DMC calculations for the Li$^+$(He)$_{20}$ clusters are reported: one clearly sees there that the radial distributions associated with the He distances from the Li$^+$ moiety show a set of more compact values related to the first shell of about 8 adatoms and a further distribution at larger distances (and broader than the first one) associated with the outer atoms that are chiefly bound by dispersion and by strongly screened induction interactions.

VI. Conclusions

In the present work we have analyzed the solvation process of a Li$^+$ ion in pure bosonic helium clusters in order to extend to a larger number of atoms the studies we had already
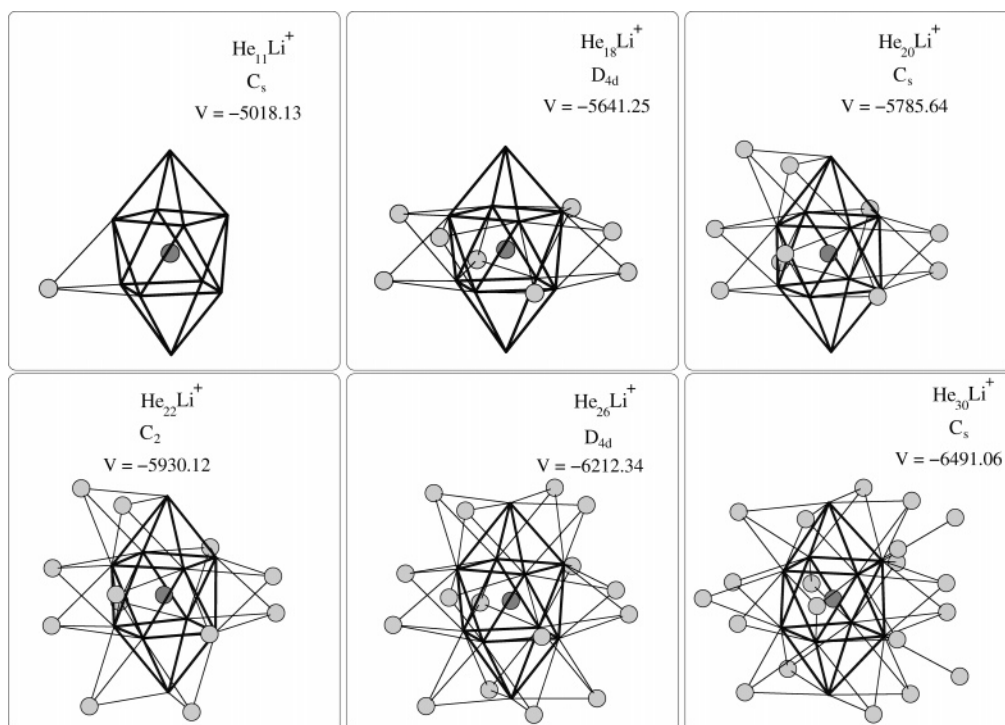

Figure 9. Optimized lowest energy structures obtained with the classical minimizations for Li$^+$He$_n$ with $n = 11$, 18, 22, 26, 30. The central polyhedron including the Li$^+$ ion represents the Li$^+$He$_{10}$ core.

Microsolvation of Li$^+$ in Small He Clusters

J. Chem. Theory Comput., Vol. 1, No. 5, 2005 **1053**

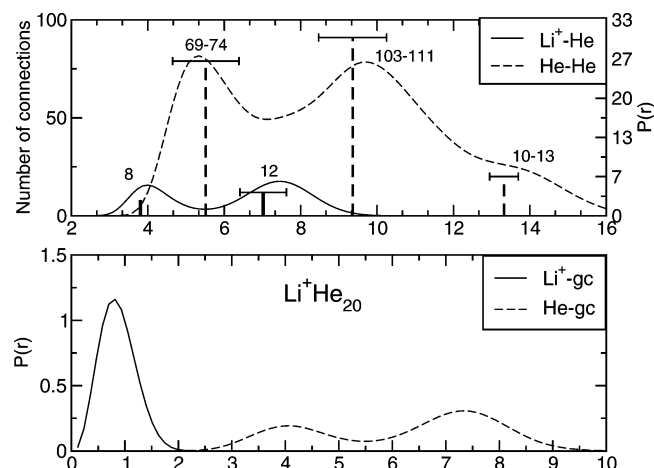**Figure 10.** Quantum DMC radial distributions for the Li$^+$He$_{20}$ moiety. Upper panel: atom−atom distance distributions compared with classical distance values as in Figure 7. Lower panel: distance distributions with respect to the geometric center of the cluster as in Figure 9.

carried out in previous work on the smaller aggregates.[1] Here a combination of classical energy minimization techniques and of "exact" quantum Monte Carlo methods have been employed in order to describe the structure and the energetics of the Li$^+$(He)$_n$ clusters with n up to 30 (20 for DMC calculations), employing always a description based on the sum-of-potential approximation.

The basic approximation which this study relies on is that of calculating the full cluster interaction as a sum of pairwise potentials. Although the error introduced by this assumption is in general found to be (in absolute terms) larger in ionic systems than in neutral ones, its relative weight remains rather small.[1] Thus, we believe that the resulting stuctures and energies would not be substantially altered by the correct use of a full many-body potential (see, for example, the discussion in ref 19 for the similar situations of H$^-$ and Cl$^-$ in Rg clusters and our calculations in ref 1).

We have therefore shown the following:

(1) The Li$^+$ is fully solvated inside larger ^{4}He clusters as already indicated by our earlier work on very small aggregates.[1]

(2) The ionic Li$^+$core does not form preferential "molecular cores" with surrounding He atoms but rather the helium adatoms remain equivalently bound within each solvation shell to the central, solvated lithium ion that persists in carrying the positive charge for more than 98%.[1]

(3) The ZPE corrections play a role in such systems, albeit strongly reduced with respect to the one found in neutral aggregates: this means that, at least in the initial solvation shell, the quantum adatoms are less delocalized and that the lithium−helium direct "bonds" are nearly rigid, classical structures.

(4) The classical optimization procedures can provide structural details which are reasonably close to those given by the quantum DMC calculations and can yield for ionic moieties the same structural picture as that given by the quantum treatment.

Furthermore, our comparison of single particle evaporation energies given by classical and quantum results suggests in both cases the formation of an initial shell of about 8 He atoms which are more strongly bound to the central ion. On the other hand, beyond that initial shell the cluster growth appears to be chiefly driven by He−He interactions, albeit at energies which are initially still kept larger than those of the neutral systems by the additional presence of the induction field due to the central ionic core. This behavior may be compared to that of Na$^+$ and K$^+$ doped helium clusters[6,7] where the first solvation shells were found to be of 9 and 12 atoms, respectively, from quantum calculations based on sum-of-potentials approximation.

References

(1) Sebastianelli, F.; Baccarelli, I.; Bodo, E.; Di Paola, C.; Gianturco, F. A.; Yurtsever, M. *J. Comput. Mater. Sci.* **2005**, in press.

(2) E.g., see: *Atomic and Molecular Beams, The state of the art 2000*; Camargue, R., Ed.; Springer: Berlin, 2000.

(3) Toennies, J. P.; Vilesov, A. F. *Angew. Chem., Int. Ed.* **2004**, *43*, 2622.

(4) Stienkemeyer, F.; Vilesov, A. F. *J. Chem. Phys.* **2001**, *115*, 10119.

(5) E.g., see: Brink, D. M.; Stringari, S. *Z. Phys. D* **1990**, *15*, 257.

(6) Galli, D. E.; Buzzacchi, M.; Reatto, L. *J. Chem. Phys.* **2001**, *115*, 10239.

(7) Rossi, M.; Verona, M.; Galli, D. E.; Reatto, L. *Phys. Rev. B* **2004**, *69*, 212510.

(8) Northby, J. *J. Chem. Phys.* **2001**, *115*, 10065.

(9) Scheidemann, A. A.; Kreisin, V. V.; Hess, H. *J. Chem. Phys.* **1997**, *107*, 2839.

(10) González-Lezana, T.; Rubayo-Soneira, J.; Miret-Artés, S.; Gianturco, F. A.; Delgado-Barrio, G.; Villarreal, P. *J. Chem. Phys.* **1999**, *110*, 9000.

(11) González-Lezana, T.; Rubayo-Soneira, J.; Miret-Artés, S.; Gianturco, F. A.; Delgado-Barrio, G.; Villarreal, P. *Phys. Rev. Lett.* **1999**, *82*, 1648.

(12) Baccarelli, I.; Delgado-Barrio, G.; Gianturco, F. A.; González-Lezana, T.; Miret-Artés, S.; Villarreal, P. *Phys. Chem. Chem. Phys.* **2000**, *2*, 4067.

(13) Gianturco, F. A.; Paesani, F.; Baccarelli, I.; Delgado-Barrio, G.; González-Lezana, T.; Miret-Artés, S.; Villarreal, P.; Bendazzoli, G. B.; Evangelisti, S. *J. Chem. Phys.* **2001**, *114*, 5520.

(14) Ceperley, D. M. *Rev. Mod. Phys.* **1995**, *67*, 279.

(15) Skullerud, H. R.; Løvaas, T. H.; Tsurugida, K. *J. Phys. B* **1999**, *32*, 4509.

Di Paola et al.

(16) Alrichs, R.; Bohm, H. J.; Brode, S.; Tang, K. T.; Toennies, J. P. *J. Chem. Phys.* **1988**, *88*, 6290.

(17) Soldan, P.; Lee, E. P. F.; Lozeille, J.; Murrel, J. N.; Wright, T. G. *Chem. Phys. Lett.* **2001**, *343*, 429.

(18) Aziz, R. A.; Slaman, M. J. *J. Chem. Phys.* **1991**, *94*, 8047.

(19) Lenzer, T.; Yourshaw, I.; Furlanetto, M. R.; Pivonka, N. L.; Neumark, D. M. *J. Chem. Phys.* **2001**, *115*, 3578.

(20) Bellert, D.; Breckenridge, W. H. *Chem. Rev.* **2002**, *102*, 1595.

(21) Wales, D. J. *J. Chem. Phys.* **1994**, *101*, 3750.

(22) Baker, J. *J. Comput. Chem.* **1986**, *7*, 385.

(23) Baker, J.; Hehre, W. H. *J. Comput. Chem.* **1991**, *12*, 606.

(24) Sebastianelli, F.; Di Paola, C.; Baccarelli, I.; Gianturco, F. A. *J. Chem. Phys.* **2003**, *119*, 8276.

(25) Sebastianelli, F.; Baccarelli, I.; Di Paola, C.; Gianturco, F. A. *J. Chem. Phys.* **2004**, *121*, 2094.

(26) Sebastianelli, F.; Baccarelli, I.; Di Paola, C.; Gianturco, F. A. *J. Chem. Phys.* **2003**, *119*, 5570.

(27) Hammond, B. L.; Lester, W. A., Jr.; Reynolds, P. J. *Monte Carlo Methods in Ab Initio Quantum Chemistry*; World Scientific: Singapore, 1994.

(28) Ceperley, D. M.; Alder, B. *Science* **1994**, *231*, 555.

(29) Suhm, M. A.; Watts, R. O. *Phys. Rev.* **1991**, *204*, 293.

(30) Lewerenz, M. J. *Chem. Phys.* **1997**, *106*, 4596.

(31) Baccarelli, I.; Gianturco, F. A.; González-Lezana, T.; Delgado-Barrio, G.; Miret-Artés, S.; Villarreal, P. *J. Chem. Phys.* **2005**, *122*, 084313.

(32) Rick, S. W.; Lynch, D. L.; Doll, J. D. *J. Chem. Phys.* **1991**, *95*, 3506.